
Continual Density Ratio Estimation in an Online Setting

Yu Chen
University of Bristol

Song Liu
University of Bristol

Tom Diethe
Amazon Research

Peter Flach
University of Bristol

Abstract

In online applications with streaming data, awareness of how far the training or test set has shifted away from the original dataset can be crucial to the performance of the model. However, we may not have access to historical samples in the data stream. To cope with such situations, we propose a novel method, Continual Density Ratio Estimation (CDRE), for estimating density ratios between the initial and current distributions (p/q_t) of a data stream in an iterative fashion without the need of storing past samples, where q_t is shifting away from p over time t . We demonstrate that CDRE can be more accurate than standard Density Ratio Estimation (DRE) in terms of estimating divergences between distributions, despite not requiring samples from the original distribution. CDRE can be applied in scenarios of online learning, such as importance weighted covariate shift, tracing dataset changes for better decision making. In addition, CDRE enables the evaluation of generative models under the setting of continual learning. To the best of our knowledge, there is no existing method that can evaluate generative models in continual learning without storing samples from the original distribution.

1 Introduction

In the real world, online applications are ubiquitous in practice since large amounts of data are generated and processed in a streaming manner. There are two types of machine learning scenarios commonly deployed for such streaming data:

- 1) train a model online on the streaming data (*e.g.* online learning (Shalev-Shwartz et al., 2012) and continual

learning (Parisi et al., 2019)) – in this case the training set may be shifting over time;

- 2) train a model offline and deploy it online – in this case the test set may be shifting over time.

In both cases, the main problem is dataset shifting, *i.e.* the data distribution changes gradually over time. Awareness of how far the training or test set has been shifted can be crucial to the performance of the model. For example, when the training set is shifting, the latest model may become less accurate on samples from earlier data distributions, like the covariate shift (Shimodaira, 2000). In this case, we can use importance weights to ‘rollback’ the model for a better prediction, where the importance weights are density ratios. In the other case, the performance of a pre-trained model may gradually degrade when the test set shifts away from the training set over time. It will be beneficial to trace the distribution difference caused by dataset shifting so that we can decide when to update the model for preventing the performance from degrading.

Density Ratio Estimation (DRE) (Sugiyama et al., 2012) is a method for estimating the ratio between two probability distributions which can reflect the difference between the two distributions. In particular, it can be applied to settings in which only samples of the two distributions are available, which is usually the case in practice. However, under certain restrictive conditions in online applications – *e.g.*, unavailability of historical samples in an online data stream – existing DRE methods are no longer applicable. Moreover, DRE exhibits difficulties for accurate estimations when there exists significant differences between the two distributions (Sugiyama et al., 2012; McAllester and Stratos, 2020; Rhodes et al., 2020). In this paper, we propose a new framework of density ratio estimation called Continual Density Ratio Estimation (CDRE) which is capable of coping with the online scenarios and gives better estimation than standard DRE when the two distributions are less similar. There are existing methods for detecting changing points online by DRE (Kawahara and Sugiyama, 2009; Liu et al., 2013; Bouchikhi et al., 2018), which estimate density ratios between distributions of two consecutive time intervals. In contrast, CDRE estimates density ratios between distributions of the initial and latest time intervals without storing historical samples.

CDRE can be applied to tracing the differences between distributions by estimating their f -divergences and thus it provides a new option for evaluating generative models in continual learning. The scenario of the training set shifting over time matches the problem setting of continual learning (Parisi et al., 2019) in which a single model is trained by a set of tasks sequentially with no (or very limited) access to the data from past tasks, and yet is able to perform on all learned tasks. The existing measures of evaluating generative models are basically to estimate the difference between the original data distribution and the distribution of model samples (Heusel et al., 2017; Bińkowski et al., 2018). All those methods require the samples from the original data distribution which may not be possible in the setting of continual learning, yet CDRE can fit in such a situation.

Our key contributions in this paper are:

- i) we propose a new framework CDRE for estimating density ratios in an online setting, which does not require storing historical samples in the data stream;
- ii) we provide an instantiation of CDRE by using Kullback-Leibler Importance Estimation Procedure (KLIEP) (Sugiyama et al., 2008) as a building block, and provide theoretical analysis of its asymptotic behaviour;
- iii) we demonstrate the efficacy of CDRE in several online applications, including backward covariate shift, tracing distribution drift, and evaluating generative models in continual learning. To the best of our knowledge, there is no prior work that can evaluate generative models in continual learning without storing samples from the original distribution.

The rest of this paper is structured as follows. Sec. 2.1 briefly reviews the formulation of KLIEP, and Sec. 2.2 introduces the problem setting of CDRE. In Sec. 3 we provide the technique details of CDRE and demonstrate the instantiation of CDRE by KLIEP. Sec. 4 introduces several applications of CDRE along with comprehensive experimental results. Finally, Sec. 5 provides some further discussion about CDRE and its applications.

2 Preliminaries

We first review the formulation of KLIEP which we use for instantiating CDRE. We then formally introduce the problem setting of CDRE.

2.1 Density Ratio Estimation by Kullback-Leibler Importance Estimation Procedure

KLIEP is a classic method for density ratio estimation introduced in Sugiyama et al. (2008). Here we review the

formulation of KLIEP because we deploy it as an example of the basic estimator of CDRE.

Let $r^*(x) = \frac{p(x)}{q(x)}$ be the (unknown) true density ratio, then $p(x)$ can be estimated by $\tilde{p}(x) = r(x)q(x)$, where $r^*(x)$ is modeled by $r(x)$. Hence, we can optimize $r(x)$ by minimizing the Kullback-Leibler (KL)-divergence between $p(x)$ and $\tilde{p}(x)$ with respect to r :

$$\begin{aligned} D_{KL}(p(x)||\tilde{p}(x)) &= \int p(x) \log \frac{p(x)}{\tilde{p}(x)} dx \\ &= \int p(x) \log r^*(x) dx - \int p(x) \log r(x) dx \end{aligned} \quad (1)$$

where $r(x)$ should satisfy $r(x) > 0$ and $\int r(x)q(x)dx = \int \tilde{p}(x)dx = 1$. As the first term of the right-hand side in Eq. (1) is constant w.r.t. $r(x)$, the empirical objective of optimizing $r(x)$ is as follows:

$$\begin{aligned} J_r &= \max_r \frac{1}{N} \sum_{i=1}^N \log r(x_i), \quad x_i \sim p(x), \\ \text{s.t. } &\frac{1}{M} \sum_{j=1}^M r(x_j) = 1, \quad r(x) \geq 0, \quad x_j \sim q(x). \end{aligned} \quad (2)$$

One convenient way of parameterizing $r(x)$ is by using a log-linear model with normalization, which then automatically satisfies the constraints in Eq. (2):

$$\begin{aligned} r(x; \beta) &= \frac{\exp(\psi_\beta(x))}{\frac{1}{M} \sum_{j=1}^M \exp(\psi_\beta(x_j))}, \\ x_j &\sim q(x), \quad \psi_\beta : \mathbb{R}^D \rightarrow \mathbb{R}, \end{aligned} \quad (3)$$

where ψ_β can be any deterministic function: we use a neural network as ψ_β in our implementations, β then representing parameters of the neural network.

2.2 The problem setting of CDRE

The goal of CDRE is estimating density ratios between two distributions $r_{\tau,t}(x) = p_\tau(x)/q_{\tau,t}(x)$, where τ is the initial time index of starting tracing a distribution, t denotes the current time index, and when $t > \tau$ the samples of $p_\tau(x)$ is unavailable. We refer to $p_\tau(x)$ as the *original distribution* and $q_{\tau,t}(x)$ as the *dynamic distribution* of $p_\tau(x)$. The dynamic distribution is assumed to be shifting away from its original distribution gradually over time. For example, let $\tau = 1$, at $t = 1$ we have access to samples of both p_τ and $q_{\tau,t}$, we can directly estimate $r_{\tau,t}$ by standard DRE, and when $t > 1$, we have no access to samples of p_τ any longer, instead, we only have access to samples of $q_{\tau,t-1}$ and $q_{\tau,t}$. CDRE is proposed to estimate $r_{\tau,t}$ in such a situation. In addition, CDRE is able to estimate ratios of multiple pairs of the original and dynamic distributions by a single estimator. It avoids building separated estimators for tracing different original distributions in an application (e.g. seasonal data), which also fits the common setting of continual learning that we will introduce in the latter sections.

3 Continual Density Ratio Estimation

In this section we introduce the basic formulation of CDRE and demonstrate instantiating it by KLIEP. For convenience, we initially introduce the formulation with a single pair of original and dynamic distributions. We then give a more general formulation for multiple pairs of original and dynamic distributions.

3.1 The basic form of CDRE

For simplicity of notation, we assume $\tau = 1$ in the case of estimating density ratios between a *single* pair of original and dynamic distributions, and then omit τ in the basic formulations. Thus, the density function of the original distribution is denoted as $p(x)$ and its samples are unavailable when $t > 1$. Similarly, $q_t(x)$ denotes the density function of the dynamic distribution at time t . The true density ratio $r_t^*(x) \triangleq p(x)/q_t(x)$ can be decomposed as follows:

$$r_t^*(x) = \frac{q_{t-1}(x)}{q_t(x)} \frac{p(x)}{q_{t-1}(x)} = r_{s_t}^*(x) r_{t-1}^*(x), \quad t > 1, \quad (4)$$

where $r_{s_t}^*(x) \triangleq q_{t-1}(x)/q_t(x)$ represents the true density ratio between the two latest dynamic distributions. Using this decomposition we can estimate $p(x)/q_t(x)$ in an iterative manner without the need of storing samples from $p(x)$ when t increases. The key point is that we can estimate $r_t^*(x)$ by estimating $r_{s_t}^*(x)$ when the estimation of $r_{t-1}^*(x)$ is known. In particular, it introduces one extra constraint:

$$\int r_{s_t}^*(x) q_t(x) dx = \int \frac{r_t^*(x)}{r_{t-1}^*(x)} q_t(x) dx = 1 \quad (5)$$

Existing methods of DRE can be applied to estimating the initial ratio $r_1^*(x) = p(x)/q_1(x)$ and the latest ratio $r_{s_t}^*(x), \forall t > 1$, as the basic ratio estimator of CDRE. Let $r_t(x)$ be the estimation of $r_t^*(x)$, where r_{t-1} is already obtained, then the objective of CDRE can be expressed as:

$$J_{CDRE}(r_t) = J_{DRE}(r_{s_t}), \quad r_{s_t}(x) \triangleq \frac{r_t(x)}{r_{t-1}(x)} \quad (6)$$

$$s.t. \quad \frac{1}{N} \sum_{n=1}^N r_{s_t}(x_n) = 1, \quad x_n \sim q_t(x).$$

where J_{DRE} can be the objective of any method used for standard DRE, such as KLIEP (Sugiyama et al., 2008).

3.2 An instantiation of CDRE: CKLIEP

We now demonstrate how to instantiate CDRE by KLIEP, which we call Continual KLIEP (CKLIEP). Define $r_t(x), r_{t-1}(x)$ by the log-linear form as in Eq. (3), let $N_t = N_{t-1} = N$ as the sample size of each distribution, then r_{s_t} is

as follows:

$$r_{s_t} = \exp\{\psi_{\beta_t}(x) - \psi_{\beta_{t-1}}(x)\} \times \frac{\frac{1}{N} \sum_{j=1}^N \exp\{\psi_{\beta_{t-1}}(x_{t-1,j})\}}{\frac{1}{N} \sum_{i=1}^N \exp\{\psi_{\beta_t}(x_{t,i})\}},$$

$$x_{t,i} \sim q_t(x), \quad x_{t-1,j} \sim q_{t-1}(x). \quad (7)$$

where β_t, β_{t-1} represent parameters of $r_t(x), r_{t-1}(x)$, respectively. When the constraint in Eq. (6) is satisfied, we have the following equality by substituting Eq. (7) into the constraint:

$$\frac{\sum_{i=1}^N \exp\{\psi_{\beta_t}(x_{t,i})\}}{\sum_{j=1}^N \exp\{\psi_{\beta_{t-1}}(x_{t-1,j})\}} = \frac{1}{N} \sum_{i=1}^N \exp\{\psi_{\beta_t}(x_{t,i}) - \psi_{\beta_{t-1}}(x_{t,i})\} \quad (8)$$

r_{s_t} can then be rewritten in the same log-linear form of Eq. (3) by substituting Eq. (8) into Eq. (7):

$$r_{s_t} = \frac{\exp\{\psi_{\beta_t}(x) - \psi_{\beta_{t-1}}(x)\}}{\frac{1}{N} \sum_{i=1}^N \exp\{\psi_{\beta_t}(x_{t,i}) - \psi_{\beta_{t-1}}(x_{t,i})\}}$$

$$= \frac{\exp\{\phi_{\beta_t}(x)\}}{\frac{1}{N} \sum_{i=1}^N \exp\{\phi_{\beta_t}(x_i)\}}, \quad (9)$$

where $\phi_{\beta_t}(x) \triangleq \psi_{\beta_t}(x) - \psi_{\beta_{t-1}}(x)$.

Now we can instantiate J_{DRE} in Eq. (6) by the objective of KLIEP (Eq. (2)) and adding the equality constraint (Eq. (8)) into the objective with a hyperparameter λ_c , which gives the objective of CKLIEP as the following:

$$\max_{\beta_t} \mathcal{L}_t(\beta_t) = \max_{\beta_t} \frac{1}{N} \sum_{j=1}^N \log r_{s_t}(x_{t-1,j})$$

$$+ \lambda_c \left(\frac{\Psi_t(x_t)}{\Phi_t(x_t) \Psi_{t-1}(x_{t-1})} - 1 \right)^2$$

where $t > 1$, $x_{t,i} \sim q_t(x)$, $x_{t-1,j} \sim q_{t-1}(x)$,

$$\Phi_t(x_t) \triangleq \frac{1}{N} \sum_{i=1}^N \exp\{\phi_{\beta_t}(x_{t,i})\}, \quad \Psi_t(x_t) \triangleq \frac{1}{N} \sum_{i=1}^N \exp\{\psi_{\beta_t}(x_{t,i})\} \quad (10)$$

where β_{t-1} is the estimated parameter of $r_{t-1}(x)$ and hence a constant in the objective.

A concurrent work (Rhodes et al., 2020) has developed Telescoping Density Ratio Estimation (TRE) by the same consecutive decomposition in Eq. (4) but with the following main differences: 1) the objective of TRE is to optimize a set of ratio estimators at the same time whereas CDRE only needs to optimize the latest ratio estimator; 2) TRE requires samples of all intermediate distributions as well as the original distribution, in contrast CDRE only requires samples of the two latest distributions.

3.3 Asymptotic normality of CKLIEP

Define $\hat{\beta}_t$ as the estimated parameter that satisfies:

$$\mathcal{L}'_t(\hat{\beta}_t) \triangleq \nabla_{\beta_t} \mathcal{L}_t(\beta_t)|_{\beta_t = \hat{\beta}_t} = 0 \quad (11)$$

Assume $\phi_{\beta_t}(x)$ (Eq. (9)) includes the correct function that there exists β_t^* recovers the true ratio over the population:

$$r_{s_t}^*(x) = \frac{q_{t-1}(x)}{q_t(x)} = \frac{\exp\{\phi_{\beta_t^*}(x)\}}{\mathbb{E}_{q_t}[\exp\{\phi_{\beta_t^*}(x)\}]}, \quad (12)$$

$$\text{where } \phi_{\beta_t^*}(x) = \Psi_{\beta_t^*}(x) - \Psi_{\beta_{t-1}}(x),$$

Notations: \rightsquigarrow and \xrightarrow{P} mean convergence in distribution and convergence in probability, respectively.

Assumptions: We assume $q_t(x)$ and $q_{t-1}(x)$ are independent, $n_t = n_{t-1} = n$, where n_t is the sample size of $q_t(x)$. Let S_t be the support of q_t , we assume $S_{t-1} \subseteq S_t$ in all cases.

Lemma 1. Let $\ell'_r(\beta_t^*) \triangleq \frac{1}{n} \sum_{j=1}^n \nabla_{\beta_t} \log r_{s_t}(x_{t-1,j})|_{\beta_t=\beta_t^*}$, we have $\sqrt{n} \ell'_r(\beta_t^*) \rightsquigarrow \mathcal{N}(0, \sigma^2)$, where

$$\sigma^2 = \text{Cov}_{q_{t-1}}[\nabla_{\beta_t} \phi_{\beta_t^*}(x)] + \frac{\text{Cov}_{q_t}[\nabla_{\beta_t} \exp\{\phi_{\beta_t^*}(x)\}]}{\mathbb{E}_{q_t}[\exp\{\phi_{\beta_t^*}(x)\}]^2}$$

Lemma 2. Let $\ell''_r(\beta_t^*) \triangleq \frac{1}{n} \sum_{j=1}^n \nabla_{\beta_t}^2 \log r_{s_t}(x_{t-1,j})|_{\beta_t=\beta_t^*}$, we have $\ell''_r(\beta_t^*) \xrightarrow{P} -I_{\beta_t^*}$, where $I_{\beta_t^*} \triangleq \text{Cov}_{q_{t-1}}[\nabla_{\beta_t} \phi_{\beta_t^*}(x)]$.

Lemma 3. Let $\ell_c(\beta_t) \triangleq \lambda_c \left(\frac{\Psi_t(x_t)}{\Phi_t(x_t)\Psi_{t-1}(x_{t-1})} - 1 \right)^2$, and $\ell'_c(\beta_t^*) \triangleq \nabla_{\beta_t} \ell_c(\beta_t)|_{\beta_t=\beta_t^*}$, if we set $\lambda_c = \frac{A}{\sqrt{n}}$, where A is a positive constant, then $\sqrt{n} \ell'_c(\beta_t^*) \xrightarrow{P} 0$.

Theorem 1. Suppose $\lambda_c = \frac{A}{\sqrt{n}}$, where A is a positive constant, assume $\ell'_c(\beta_t^*) = o_p(1)$, $\hat{\beta}_t - \beta_t^* = o_p(1)$, $\mathcal{L}_t'''(\tilde{\beta}_t) = O_p(1)$, where $\tilde{\beta}_t$ is a point between $\hat{\beta}_t$ and β_t^* , then $\sqrt{n}(\hat{\beta}_t - \beta_t^*) \rightsquigarrow \mathcal{N}(0, v^2)$, where

$$v^2 = I_{\beta_t^*}^{-1} + \mathbb{E}_{q_t}[\exp\{\phi_{\beta_t^*}(x)\}]^{-2} \times I_{\beta_t^*}^{-1} \text{Cov}_{q_t}[\nabla_{\beta_t} \exp\{\phi_{\beta_t^*}(x)\}] I_{\beta_t^*}^{-1} \quad (13)$$

Corollary 1. Suppose $p(x)$ and $\forall t, q_t(x)$ are from the exponential family, define $r_{s_t}^*(x) = \exp\{\phi_{\beta_t^*}(x)\}$, $\phi_{\beta_t^*}(x) = \beta_t^* T(x) + C$, $T(x)$ is a sufficient statistic of x , C is a constant, then $\sqrt{n}(\hat{\beta}_t - \beta_t^*) \rightsquigarrow \mathcal{N}(0, v_e^2)$, where $T(x)$ is a column vector, $T(x)^2 = T(x)T(x)^T$, $I_{\beta_t^*} = \text{Cov}_{q_{t-1}}[T(x)]$:

$$v_e^2 = I_{\beta_t^*}^{-1} + I_{\beta_t^*}^{-1} (\mathbb{E}_{q_{t-1}}[r_{s_t}^*(x)T(x)^2] - \mathbb{E}_{q_{t-1}}[T(x)]^2) I_{\beta_t^*}^{-1} \quad (14)$$

All proofs are provided in Appx. A. Corollary 1 shows that how the covariance matrix v_e^2 depends on the latest density ratio ($r_{s_t}^*$) when the distributions are from the exponential family. Since a smaller variance is better for convergence, we would prefer $r_{s_t}^*(x) = q_{t-1}(x)/q_t(x)$ is small, which means when $q_{t-1}(x)$ is large $q_t(x)$ should be also large. In this case, $r_{s_t}^*$ is less likely to explode and the variance of the estimated parameter would be likely confined. We demonstrate this by experiments with 1-D Gaussian distributions. We fix $q_{t-1}(x) = \mathcal{N}(0, 1)$, setting $q_t(x) =$

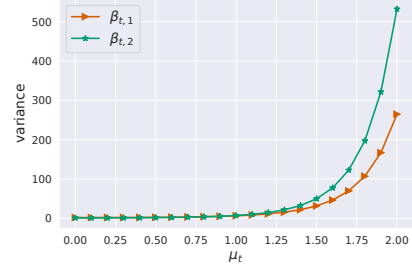


Figure 1: Demonstration of the variance of estimated parameters in Corollary 1 by 1-D Gaussian distributions: fix $q_{t-1}(x) = \mathcal{N}(0, 1)$ and $q_t(x) = \mathcal{N}(\mu_t, 1)$.

$\mathcal{N}(\mu_t, 1)$, where $\mu_t = \delta k$, $\delta = 0.1$, $k \in \{0, 1, \dots, 20\}$. In this case, $T(x) = \{x, x^2\}$, $\beta_t = \{\beta_{t,1}, \beta_{t,2}\}$, we display the diagonal of v_e^2 (variance of $\beta_{t,1}, \beta_{t,2}$) in Fig. 1. It is clear that when q_t is farther to q_{t-1} , the variance is larger.

When $\beta_t = \beta_t^*$, $n \rightarrow \infty$, we have $r_t(x) = r_{s_t}^*(x)r_{t-1}(x)$, then $\log r_t^*(x) - \log r_t(x) = \log r_{t-1}^*(x) - \log r_{t-1}(x)$, which means the error inherited from $r_{t-1}(x)$ will be the intrinsic error for estimating $r_t^*(x)$ due to the objective of CDRE is iterative. It indicates that smaller difference between each intermediate q_τ and $q_{\tau-1}$ ($\forall 1 < \tau \leq t$) leads to a better estimation. We demonstrate in Sec. 4.2 that it is often the case in practice even when $\Psi_{\beta_t^*}(x)$ is approximated by a non-linear model. Moreover, Fig. 1 shows the variance of the estimation may grow rapidly when the difference between the two distributions exceeds a certain value. CKLIEP can prevent such an issue by ensuring the difference between any intermediate pairs of distributions is relatively small. We will demonstrate this in Sec. 4.2 as well.

3.4 Multiple original distributions in CDRE

Now we consider tracing multiple original distributions in CDRE, in which case a new pair of original and dynamic distributions will be added into the training process of the estimator at some time point. We refer to an original distribution as $p_\tau(x)$, where τ is the time index of starting tracing the original distribution. And samples of $p_\tau(x)$ are not available when $t > \tau$. Similarly, $q_{\tau,t}(x)$ denotes the dynamic distribution that corresponding to $p_\tau(x)$ at time t :

$$r_{\tau,t}^*(x) = \frac{p_\tau(x)}{q_{\tau,t}(x)} = \frac{q_{\tau,t-1}(x)}{q_{\tau,t}(x)} \frac{p_\tau(x)}{q_{\tau,t-1}(x)} = r_{s_{\tau,t}}^*(x) r_{\tau,t-1}^*(x),$$

Where $r_{s_{\tau,t}}^*(x) = q_{\tau,t-1}(x)/q_{\tau,t}(x)$. In this case, we optimize the estimator at time t by an averaged objective:

$$\max_{\beta_t} \bar{\mathcal{L}}_t(\beta_t) = \max_{\beta_t} \frac{1}{|\mathbb{T}|} \sum_{\tau \in \mathbb{T}} \mathcal{L}_t(\beta_t; \tau) \quad (15)$$

where \mathbb{T} is the set of time indices of adding original distributions, $|\mathbb{T}|$ is the size of \mathbb{T} . $\mathcal{L}_t(\beta_t; \tau)$ is as the same as the loss function of a single original distribution (Eq. (10)) for

a given τ . Further, $r_{s_{\tau,t}}(x)$ is also defined by the same form of Eq. (9), the difference is that $\psi_{\beta_t}(x)$ becomes $\psi_{\beta_t}(x; \tau)$. In our implementation, we concatenate the time index τ to each data sample as the input of the ratio estimator. Thus, we can avoid learning separate ratio estimators for multiple original distributions. In addition, we set the output of $\psi_{\beta_t}(\cdot)$ as a $|\mathbb{T}|$ -dimensional vector $\{o_1, \dots, o_i, \dots, o_{|\mathbb{T}|}\}$ where o_i corresponds to the output of $\psi_{\beta_t}(x; \tau = \mathbb{T}_i)$. Note that with CDRE we have the flexibility to extend the model architecture since the latest estimator function ϕ_{β_t} only needs the output of the previous estimator function $\psi_{\beta_{t-1}}$. This can be beneficial when the model capacity becomes a bottleneck of the performance.

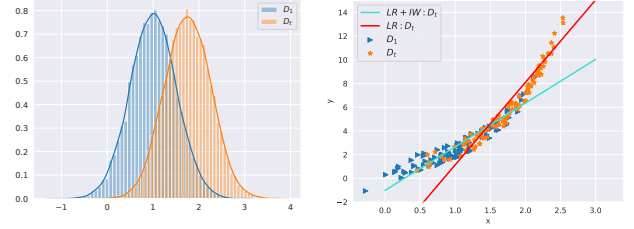
3.5 Dimensionality reduction in online applications

The main concern of estimating density ratios stems from high-dimensional data. Several methods for dimensionality reduction in DRE have been introduced in (Sugiyama et al., 2012). A fundamental assumption of these methods is that the difference between two distributions can be confined to a subspace, which means $p(z)/q(z) = p(x)/q(x)$ where z is a lower-dimensional representation of x . This aims for exact density ratio estimation in a subspace but incurs a high computational cost. In most applications, a model (e.g. classifiers) is often trained upon a representation extractor, indicating a surrogate feature space of high-dimensional data can be used for the density ratio estimation in practice. For instance, most measurements of generative models estimate the difference between two distributions in a surrogate feature space, e.g., the inception feature defined for the Inception Score (IS) (Salimans et al., 2016) is extracted by a neural network, and this method is also applied in many other measurements of generative models, e.g. Fréchet Inception Distance (FID) (Heusel et al., 2017), Kernel Inception Distance (KID) (Bińkowski et al., 2018).

In prior work, a pre-trained classifier is often used to generate surrogate features of high-dimensional image data (e.g. inception features (Salimans et al., 2016)). However, it may be difficult to train such a classifier in online applications because: a) a homogeneous dataset for all unseen data or tasks may not be available in advance; b) labeled data may not be available in generative tasks. In order to cope with such circumstances, we introduce Continual Variational Auto Encoder (CVAE) in a pipeline with CDRE. The loss function of CVAE is defined as the following:

$$\begin{aligned} \mathcal{L}_{CVAE}(\theta_t, \vartheta_t) &= NLL + \mathcal{D}_{KL}(q_t(z) || q_{t-1}(z)), \\ NLL &= -\frac{1}{t} \left[\sum_{\tau=1}^{t-1} \mathbb{E}_{q_{\tau,t-1}(x)} [\mathbb{E}_{q_t(z)} [\log p(x|z; \vartheta_t)]] \right. \\ &\quad \left. + \mathbb{E}_{p_t(x)} [\mathbb{E}_{q_t(z)} [\log p(x|z; \vartheta_t)]] \right] \end{aligned} \quad (16)$$

where $q_t(z) = \mathcal{N}(\mu_{\theta_t}(x), \sigma_{\theta_t}(x))$, θ_t and ϑ_t denote parameters of the encoder and decoder of CVAE, respectively.



(a) data distribution at $\tau = 1$ (b) Linear regression trained by (D_1) and $\tau = t$ (D_t)
(D_1) and $\tau = t$ (D_t)

Figure 2: Demo experiment of backward covariate shift. (a) shows the data distribution of training set at $\tau = 1$ and $\tau = t$. (b) displays the regression lines learnt by the model at $\tau = t$, the cyan and red lines are fitted by D_t with and without importance weights, respectively.

NLL is the negative log likelihood term as the same as in vanilla VAE (Kingma and Welling, 2013), the training data set includes samples of all dynamic distributions at the previous step ($q_{\tau,t-1}(x), \forall \tau < t$) and the samples of the current original distribution ($p_t(x)$). The KL-divergence term in the loss function serves a regularization term: the current encoder is expected to give similar z for a similar x comparing with the previous encoder. This term forces the consistency between inputs of the previous and current ratio estimators (i.e. inputs of $\psi_{\beta_{t-1}}$ and ψ_{β_t} in Eq. (10)). CVAE can generate effective features without requiring labels or pre-training, nevertheless, other commonly used methods (e.g. pre-trained classifiers) are also applicable to CDRE.

4 Applications

In this section we introduce several applications of CDRE: 1) backwards covariate shift; 2) tracing distribution shifts by KL-divergence; 3) evaluating generative models in continual learning. We demonstrate the efficacy of CDRE by comprehensive experiments. The standard deviation of all results are from 10 runs with different random seeds. In all of our experiments, $\psi(\cdot)$ is a neural network with two dense layers, each having 256 hidden units and ReLU activations. We provide more details of the experiments in the supplementary material.

4.1 Backwards covariate shift

We demonstrate that CDRE can be applied in *backward covariate shift* in which case the training set is shifting and the test set is from a previous distribution. It just swaps the situation of training and test set in common covariate shift (Sugiyama et al., 2008; Shimodaira, 2000). We assume a linear regression model defined as $\hat{y} = wx + b + \epsilon_0$, where the noise $\epsilon_0 \sim \mathcal{N}(0, 0.01)$. At time τ , the training data $x \in D_\tau$ and D_τ is shifting away from D_1 gradually, where $\tau \in \{1, 2, \dots, t\}$ and $t = 10$ is the latest time index. Fig. 2a

displays the data distribution at time $\tau = 1$ and $\tau = t$ in which we can see there exists notable difference between the two distributions. When the model is trained by D_t , it will not be able to accurately predict on test samples from D_1 unless we adjust the loss function by importance weights (i.e. density ratios) as in handling covariate shift:

$$\mathcal{L} = \mathbb{E}_{x \sim q_t(x)} \left[\frac{q_1(x)}{q_t(x)} (y - \hat{y})^2 \right]$$

Fig. 2b shows the regression lines learned by the model at $\tau = t$ with and without the importance weights, where the weights $q_1(x)/q_t(x)$ are estimated by CKLIEP. We can see that the line learned with importance weights fits D_1 more accurately than the one without the weights. This enables the model to make reasonable predictions on test samples from D_1 when the training set of D_1 is not available.

4.2 Tracing distribution shifts via KL-divergence

By estimating density ratios, we can approximate f -divergences between two distributions:

$$\mathcal{D}_f(p||q) = \mathbb{E}_q \left[f \left(\frac{p(x)}{q(x)} \right) \right] \approx \frac{1}{N} \sum_{i=1}^N f(r(x_i)) \quad (17)$$

where $x_i \sim q(x)$, $f(\cdot)$ is a convex function and $f(1) = 0$. Thus, we can trace the distribution shifts by using CDRE to approximate the f -divergences between $p_\tau(x)$ and $q_{\tau,t}(x)$ in the online setting described in Sec. 2.2. In our implementations, we apply CKLIEP to instantiate CDRE and choose the KL-divergence (i.e. setting $f(r) = -\log(r)$) to instantiate f -divergences. We compare the performance of CKLIEP with KLIEP and true values using synthetic Gaussian data, where KLIEP has access to samples of all original distributions at all time. The sample size of each distribution in the experiments is 50000.

We first simulate the scenario of a single original distribution which is a 64-D Gaussian distribution $p(x) = \mathcal{N}(\mu_0, \sigma_0^2 I)$, where $\mu_0 = 0, \sigma_0 = 1$. At each time step, we shift the distribution by a constant change on its mean and variance: $q_t(x) = \mathcal{N}(\mu_t, \sigma_t^2 I), \mu_t = \mu_0 + \Delta\mu * k, \sigma_t = \sigma_0 - \Delta\sigma * k, \Delta\mu = \Delta\sigma = 0.02, k$ is the number of time steps within one estimation interval. We set the total number of time steps to 20. We estimate $p(x)/q_t(x)$ by applying CKLIEP with two different time intervals: (1). CKLIEP-d1 is to estimate $p(x)/q_t(x)$ at each time step, i.e. $k = 1$; (2). CKLIEP-d4 is to estimate $p(x)/q_t(x)$ at every four time steps, i.e. $k = 4$. We compare the MAE of log ratios ($mae = \frac{1}{N} \sum_{n=1}^N |\log r^*(x_n) - \log \hat{r}(x_n)|$) estimated by CKLIEP and KLIEP in Fig. 3a, and compare the estimated KL-divergence with the true value in Fig. 3b. According to Corollary 1, the difference between $q_{t-1}(x)$ and $q_t(x)$ plays an important role in the estimation convergence, which explains why CKLIEP-d4 gets worse performance than CKLIEP-d1. KLIEP can be viewed as a special case

of CKLIEP when $q_{t-1}(x) = p(x)$, so the difference between $p(x)$ and $q_t(x)$ is critical to its convergence as well. We can see that in Figs. 3a and 3b KLIEP has become much worse at the last two steps due to the two distributions are too far away from each other and thus causes serious difficulties in its convergence with a fixed sample size.

We also simulate the scenario of multiple original distributions by 64-D Gaussian data: $p_\tau(x) = \mathcal{N}(\mu_\tau, \sigma_\tau^2 I)$, where $\tau \in \{1, 2, \dots, 10\}, \mu_\tau = 2\tau, \sigma_\tau = 1$. We shift each joined original distribution ($p_\tau(x), \forall \tau < t$) by a constant change as the single pair scenario and set $k = 1, \Delta\mu = \Delta\sigma = 0.01$, and add a new original distribution ($p_t(x)$) at each time step. In Fig. 3c, we compare the averaged KL-divergences ($\bar{\mathcal{D}} = \frac{1}{t} \sum_{\tau=1}^t \mathcal{D}_{KL}(q_{\tau,t}||p_\tau)$) estimated by CKLIEP and KLIEP with the true value. CKLIEP outperforms KLIEP when t increases, which aligns with the scenario of a single original distribution.

4.3 Evaluating generative models in continual learning by f -divergences

Evaluating a generative model in continual learning can be viewed as a special case of multiple original distributions of CDRE. A simplified scenario for generative models in continual learning is depicted in Fig. 4, where the goal is to learn a generative model for one category (digit) per task while it still be able to generate samples of all previous categories. The training dataset of task t consists of real samples of category t and samples of task $1 \dots t - 1$ generated by the previous model. The task index can be treated as the time index, the data distribution of the task τ can be viewed as a new original distribution $p_\tau(x)$ that added at time τ , and its corresponding dynamic distribution $q_{\tau,t}(x)$ is the sample distribution generated by the model after trained on task t . The goal of generative models in continual learning is to make $q_{\tau,t}(x)$ as close to $p_\tau(x)$ as possible. In the sense of measuring the difference between $q_{\tau,t}(x)$ and $p_\tau(x)$, we can evaluate a generative model in continual learning by estimating the averaged f -divergences over all learned tasks:

$$\bar{\mathcal{D}}_t = \frac{1}{t} \sum_{\tau=1}^t \mathbb{E}_{q_{\tau,t}} [f(r_{\tau,t}(x))] \approx \frac{1}{t} \sum_{\tau=1}^t \sum_{n=1}^{N_\tau} f(r_{\tau,t}(x_n))$$

Estimating f -divergences using density ratios has been well studied (Kanamori et al., 2011; Nguyen et al., 2010). Although the density ratio can also be estimated by the density functions of distributions, explicit density functions are often not available in practice. In the absence of prior work on evaluating generative models by f -divergences, we provide experimental results in the supplementary material for demonstrating differences between f -divergences, FID, KID, and Precision and Recall for Distributions (PRD) (Sajjadi et al., 2018). Through these experiments, we show that f -divergences can be alternative measures of generative models and one may obtain richer criteria by them.

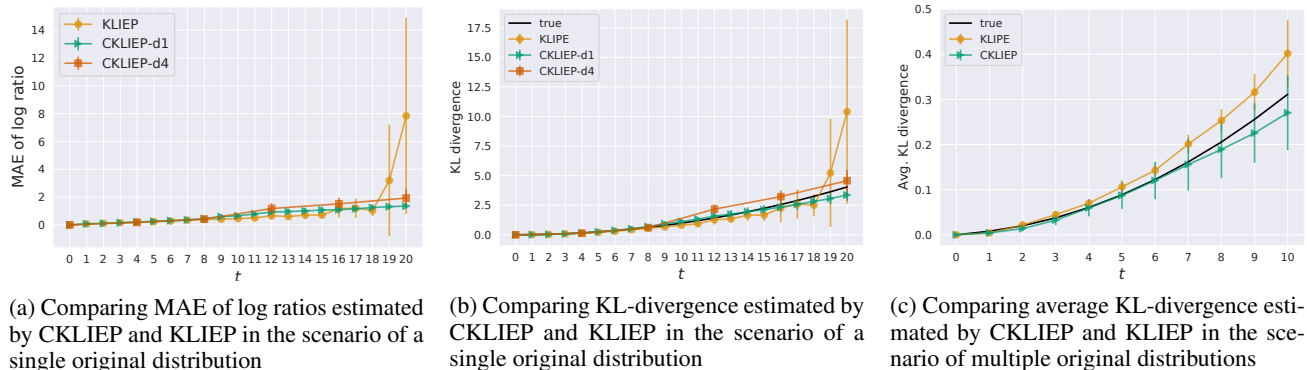


Figure 3: Comparing the performance of CKLIEP and KLIEP by synthetic data in the scenarios of the single and multiple original distributions. (a) & (b) compare the Mean Absolute Error (MAE) of log ratios and estimated KL-divergences for a single original distribution, (c) compares the average KL-divergences for multiple original distributions. The true values of KL-divergences are computed by true ratios. The error bar is the standard deviation of 10 runs.

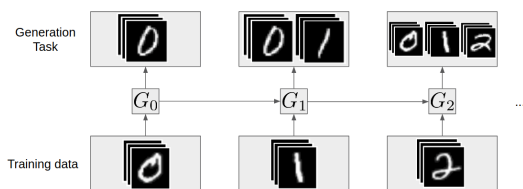


Figure 4: Demonstration of generative models in continual learning. At task t the training set consists of samples of category $t - 1$ and samples generated by the model at the previous task, and the model is to generate samples from all previously seen categories (figure reproduced from Lesort et al. (2018)).

In our experiments, the evaluated Generative Adversarial Networks (GANs) include WGAN (Arjovsky et al., 2017), WGAN-GP (Gulrajani et al., 2017), and two members of f -GANs (Nowozin et al., 2016): f -GAN-rvKL and f -GAN-JS, which instantiate the f -GAN by reverse KL and Jensen-Shannon divergences respectively. All GANs are tested as conditional GANs (Mirza and Osindero, 2014) using task indices as conditioners, and one task includes a single class of the data. We trained the GANs on Fashion-MNIST (Xiao et al., 2017). The sample size is 6000 for each class. More details of the experimental settings and the extra results with MNIST (LeCun et al., 2010) are provided in the supplementary material. We evaluate these GANs in continual learning by a few members of f -divergences which are estimated by CKLIEP, and compare the results with common measures FID, KID as used in static learning.

We deployed two feature generators in the experiments: 1) A classifier pre-trained on real samples of all classes, which is a Convolutional Neural Network (CNN) and the extracted features are the activations of the last hidden layer (similar with inception feature); 2) A CVAE trained along with the procedure of continual learning, and the

features are the output of the encoder. The dimension of features are 64 for both classifier and CVAE. We deployed the pre-trained classifier as the feature generator for FID, KID, and deployed the CVAE as the feature generator for CKLIEP in all experiments. Fig. 5 compares the evaluations for the GANs by FID, KID, and four members of f -divergences (which are estimated by CKLIEP): KL, reverse KL, Jensen-Shannon, Hellinger. All these measures are the lower the better. We also display randomly chosen samples generated by those GANs in Fig. 6 for a better understanding of the evaluations.

In general, all measurements give similar evaluations. For example, f -GAN-rvKL has the worst performance on all measures during the whole task sequence, whereas WGAN and WGAN-GP have similar performance on all measures. One main disagreement is that f -GAN-JS shows a decreasing trend on FID and KID but shows a slightly increasing trend on members of f -divergences. According to displayed samples of f -GAN-JS (Fig. 6c), there is no notable improvement observed while f -GAN-JS learning more tasks, hence, the evaluations given by FID and KID are doubtful in this case. Moreover, KID also shows doubtful evaluations for WGAN and WGAN-GP. Visually, samples from WGAN and WGAN-GP (Figs. 6a and 6b) are obviously losing fidelity while learning more tasks, which matches the increasing trend in all measures except KID. In principle, f -divergences may have different opinions with FID and KID because f -divergences are based on density ratios which may give more attention on parts with less probability mass (due to the ratio of two small values can be very large) whereas FID and KID are based on Integral Probability Metrics (IPM) (Sriperumbudur et al., 2012) which focus on parts of the distribution with most probability mass. We illustrate this by a demo experiment in the supplementary material. All in all, these experimental results demonstrate that f -divergences estimated by CKLIEP can provide meaningful evaluations for generative

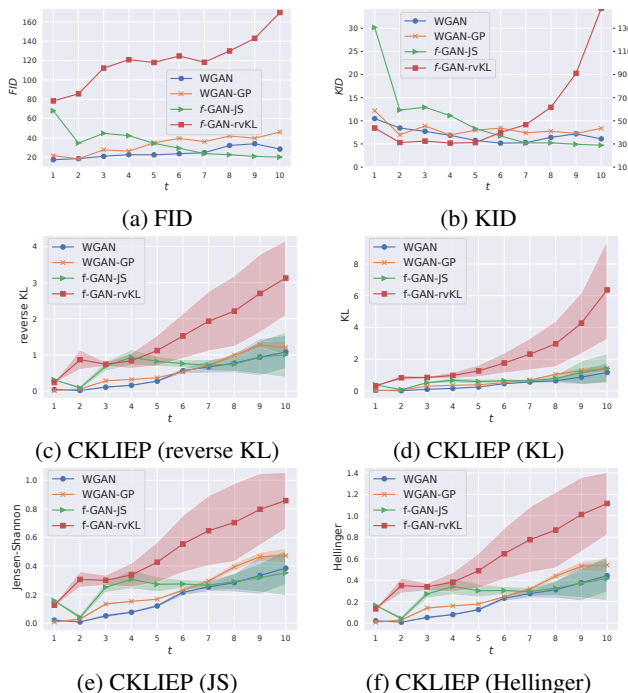


Figure 5: Evaluating GANs in continual learning on Fashion-MNIST. The shaded area are plotted by standard deviation of 10 runs. The x-axis is task index and y-axis is the specified measurement as in each sub-caption. The y-axis in the right side of Fig. 5b is the y-axis of the red line (f -GAN-rvKL), which is in a much larger scale than others. All the measures are the lower the better.

models in continual learning.

5 Conclusion and discussion

We proposed a novel method CDRE for estimating density ratios in an online setting. We demonstrate the efficacy of our method in a range of online applications, such as tracing distribution shifts by KL-divergence, backwards covariate shift, evaluating generative models in continual learning. The experiments showed that it can obtain better performance than common DRE methods without the need of storing historical samples in the streaming data. We also demonstrated that CDRE can provide an alternative approach for model selection in continual learning when other measures are not applicable. In addition, we proposed a simple approach CVAE for feature generation in continual learning when a pre-trained classifier is not available. Our experiments showed that CDRE combined with CVAE can work well on high-dimensional data, which is a difficult scenario for density ratio estimation.

When estimating divergences which are not based on log-ratios it may be better try some other form of ratio estimators (*i.e.* replacing KLIEP’s formulation). For instance,

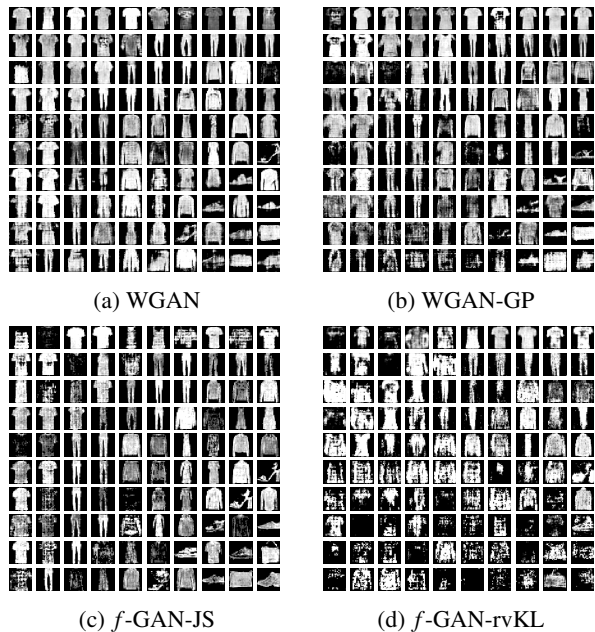


Figure 6: Fashion-MNIST samples generated by several GANs in continual learning. In each sub-figure, each row displays images generated by the model at each task, the order is from the top to bottom (task 1 to 10). The generated samples are from all learned classes at task i . The displayed samples are uniformly randomly chosen from generated samples of each class.

it may be preferable to use Least-Squares Importance Fitting (LSIF) (Kanamori et al., 2009) when estimating Pearson χ^2 divergence, since a small deviation in log-ratio can result in large squared errors. Also, since LSIF itself is based on Pearson χ^2 divergence, it appears to be a more natural choice. On the other hand, it has been discussed in Mohamed and Lakshminarayanan (2016) that the discriminator of some type of GANs can be viewed as a density ratio estimator. For instance, it is feasible to apply the formulation of the discriminators of f -GAN (Nowozin et al., 2016) to the basic estimator in CDRE. We plan to explore further possibilities of CDRE. It is also possible to estimate the Bregman divergence by ratio estimation (Uehara et al., 2016), giving even more options for the online applications of CDRE. DRE also has many other applications other than estimating divergences, such as change detection (Liu et al., 2013) and mutual information estimation (Sugiyama et al., 2012). Likewise, CDRE may be useful for more applications in the online setting which we would like to explore in the future. Finally, we mention CDRE’s potential to estimating ratios when the difference between the two distributions is significant by accompanying with methods for sampling intermediate distributions, e.g. the one introduced in Rhodes et al. (2020).

References

- Arjovsky, M., Chintala, S., and Bottou, L. (2017). Wasserstein generative adversarial networks. In *International Conference on Machine Learning*, pages 214–223.
- Bińkowski, M., Sutherland, D. J., Arbel, M., and Gretton, A. (2018). Demystifying MMD GANs. In *International Conference on Learning Representations (ICLR)*.
- Bouchikhi, I., Ferrari, A., Richard, C., Bourrier, A., and Bernot, M. (2018). Non-parametric online change-point detection with kernel lms by relative density ratio estimation. In *2018 IEEE Statistical Signal Processing Workshop (SSP)*, pages 538–542. IEEE.
- Gulrajani, I., Ahmed, F., Arjovsky, M., Dumoulin, V., and Courville, A. C. (2017). Improved training of Wasserstein GANs. In *Advances in Neural Information Processing Systems*, pages 5767–5777.
- Heusel, M., Ramsauer, H., Unterthiner, T., Nessler, B., and Hochreiter, S. (2017). GANs trained by a two time-scale update rule converge to a local Nash equilibrium. In *Advances in Neural Information Processing Systems*, pages 6626–6637.
- Kanamori, T., Hido, S., and Sugiyama, M. (2009). Efficient direct density ratio estimation for non-stationarity adaptation and outlier detection. In *Advances in neural information processing systems*, pages 809–816.
- Kanamori, T., Suzuki, T., and Sugiyama, M. (2011). f -divergence estimation and two-sample homogeneity test under semiparametric density-ratio models. *IEEE Transactions on Information Theory*, 58(2):708–720.
- Karras, T., Laine, S., and Aila, T. (2019). A style-based generator architecture for generative adversarial networks. In *Proceedings of the IEEE Conference on Computer Vision and Pattern Recognition*, pages 4401–4410.
- Kawahara, Y. and Sugiyama, M. (2009). Change-point detection in time-series data by direct density-ratio estimation. In *Proceedings of the 2009 SIAM International Conference on Data Mining*, pages 389–400. SIAM.
- Kingma, D. P. and Welling, M. (2013). Auto-encoding variational Bayes. *arXiv preprint arXiv:1312.6114*.
- LeCun, Y., Cortes, C., and Burges, C. (2010). MNIST handwritten digit database. *AT&T Labs [Online]*. Available: <http://yann.lecun.com/exdb/mnist>, 2:18.
- Lesort, T., Caselles-Dupré, H., Garcia-Ortiz, M., Stoian, A., and Filliat, D. (2018). Generative models from the perspective of continual learning. *arXiv preprint arXiv:1812.09111*.
- Liu, S., Yamada, M., Collier, N., and Sugiyama, M. (2013). Change-point detection in time-series data by relative density-ratio estimation. *Neural Networks*, 43:72–83.
- McAllester, D. and Stratos, K. (2020). Formal limitations on the measurement of mutual information. In *International Conference on Artificial Intelligence and Statistics*, pages 875–884.
- Mirza, M. and Osindero, S. (2014). Conditional generative adversarial nets. *arXiv preprint arXiv:1411.1784*.
- Mohamed, S. and Lakshminarayanan, B. (2016). Learning in implicit generative models. *arXiv preprint arXiv:1610.03483*.
- Nguyen, X., Wainwright, M. J., and Jordan, M. I. (2010). Estimating divergence functionals and the likelihood ratio by convex risk minimization. *IEEE Transactions on Information Theory*, 56(11):5847–5861.
- Nowozin, S., Cseke, B., and Tomioka, R. (2016). f-GAN: Training generative neural samplers using variational divergence minimization. In *Advances in Neural Information Processing Systems*, pages 271–279.
- Parisi, G. I., Kemker, R., Part, J. L., Kanan, C., and Wermter, S. (2019). Continual lifelong learning with neural networks: A review. *Neural Networks*.
- Rhodes, B., Xu, K., and Gutmann, M. U. (2020). Telescoping density-ratio estimation. *NeurIPS*.
- Sajjadi, M. S., Bachem, O., Lucic, M., Bousquet, O., and Gelly, S. (2018). Assessing generative models via precision and recall. In *Advances in Neural Information Processing Systems*, pages 5228–5237.
- Salimans, T., Goodfellow, I., Zaremba, W., Cheung, V., Radford, A., and Chen, X. (2016). Improved techniques for training GANs. In *Advances in neural information processing systems*, pages 2234–2242.
- Shalev-Shwartz, S. et al. (2012). Online learning and online convex optimization. *Foundations and Trends® in Machine Learning*, 4(2):107–194.
- Shimodaira, H. (2000). Improving predictive inference under covariate shift by weighting the log-likelihood function. *Journal of statistical planning and inference*, 90(2):227–244.
- Sriperumbudur, B. K., Fukumizu, K., Gretton, A., Schölkopf, B., Lanckriet, G. R., et al. (2012). On the empirical estimation of integral probability metrics. *Electronic Journal of Statistics*, 6:1550–1599.
- Sugiyama, M., Suzuki, T., and Kanamori, T. (2012). *Density ratio estimation in machine learning*. Cambridge University Press.
- Sugiyama, M., Suzuki, T., Nakajima, S., Kashima, H., von Büna, P., and Kawanabe, M. (2008). Direct importance estimation for covariate shift adaptation. *Annals of the Institute of Statistical Mathematics*, 60(4):699–746.
- Uehara, M., Sato, I., Suzuki, M., Nakayama, K., and Matsuo, Y. (2016). Generative adversarial nets from a density ratio estimation perspective. *arXiv preprint arXiv:1610.02920*.

Xiao, H., Rasul, K., and Vollgraf, R. (2017). Fashion-MNIST: a novel image dataset for benchmarking machine learning algorithms.

Xu, B., Wang, N., Chen, T., and Li, M. (2015). Empirical evaluation of rectified activations in convolutional network. *arXiv preprint arXiv:1505.00853*.

A Proof of asymptotic normality of CKLIEP

Define $\hat{\beta}_t$ as the estimated parameter that satisfies:

$$\mathcal{L}'_t(\hat{\beta}_t) \triangleq \nabla_{\beta_t} \mathcal{L}_t(\beta_t)|_{\beta_t=\hat{\beta}_t} = 0 \quad (18)$$

Assume $\phi_{\beta_t}(x)$ ($\phi_{\beta_t}(x) = \psi_{\beta_t}(x) - \psi_{\beta_{t-1}}(x)$) includes the correct function that there exists β_t^* recovers the true ratio over the population:

$$r_{s_t}^*(x) = \frac{q_{t-1}(x)}{q_t(x)} = \frac{\exp\{\phi_{\beta_t^*}(x)\}}{\mathbb{E}_{q_t}[\exp\{\phi_{\beta_t^*}(x)\}]}, \quad (19)$$

where $\phi_{\beta_t^*}(x) = \psi_{\beta_t^*}(x) - \psi_{\beta_{t-1}}(x)$,

Notations: \rightsquigarrow and \xrightarrow{P} mean convergence in distribution and convergence in probability, respectively.

Assumptions: We assume $q_t(x)$ and $q_{t-1}(x)$ are independent, $n_t = n_{t-1} = n$, where n_t is the sample size of $q_t(x)$. Let S_t be the support of q_t , we assume $S_{t-1} \subseteq S_t$ in all cases.

Lemma 4. Let $\ell'_r(\beta_t^*) \triangleq \frac{1}{n} \sum_{j=1}^n \nabla_{\beta_t} \log r_{s_t}(x_{t-1,j})|_{\beta_t=\beta_t^*}$, we have $\sqrt{n} \ell'_r(\beta_t^*) \rightsquigarrow \mathcal{N}(0, \sigma^2)$, where

$$\sigma^2 = Cov_{q_{t-1}}[\nabla_{\beta_t} \phi_{\beta_t^*}(x)] + \frac{Cov_{q_t}[\nabla_{\beta_t} \exp\{\phi_{\beta_t^*}(x)\}]}{\mathbb{E}_{q_t}[\exp\{\phi_{\beta_t^*}(x)\}]^2}$$

Proof. Because

$$\nabla_{\beta_t} \log r_{s_t}(x) = \nabla_{\beta_t} \phi_{\beta_t}(x) - \frac{\sum_i^n \nabla_{\beta_t} \exp\{\phi_{\beta_t}(x_{t,i})\}}{\sum_i^n \exp\{\phi_{\beta_t}(x_{t,i})\}} \quad (20)$$

then

$$\begin{aligned} \sqrt{n} \ell'_r(\beta_t) &= \frac{\sqrt{n}}{n} \sum_{j=1}^n \nabla_{\beta_t} \phi_{\beta_t}(x_{t-1,j}) - \\ &\quad \frac{\frac{1}{n} \sum_i^n \nabla_{\beta_t} \exp\{\phi_{\beta_t}(x_{t,i})\}}{\frac{1}{n} \sum_i^n \exp\{\phi_{\beta_t}(x_{t,i})\}} \end{aligned} \quad (21)$$

By the central limit theorem we have:

$$\begin{aligned} \frac{1}{n} \sum_{j=1}^n \nabla_{\beta_t} \phi_{\beta_t}(x_{t-1,j}) &\rightsquigarrow \mathcal{N}\left(\mathbb{E}_{q_{t-1}}[\nabla_{\beta_t} \phi_{\beta_t}(x)], \frac{Cov_{q_{t-1}}[\nabla_{\beta_t} \phi_{\beta_t}(x)]}{n}\right), \\ \frac{1}{n} \sum_i^n \nabla_{\beta_t} \exp\{\phi_{\beta_t}(x_{t,i})\} &\rightsquigarrow \\ &\quad \frac{\mathbb{E}_{q_t}[\nabla_{\beta_t} \exp\{\phi_{\beta_t}(x_{t,i})\}]}{\mathbb{E}_{q_t}[\exp\{\phi_{\beta_t}(x_{t,i})\}]} \\ &\quad + \mathbb{E}_{q_{t-1}}[(\nabla_{\beta_t} \phi_{\beta_t}(x))^2] \end{aligned} \quad (22)$$

and by the weak law of large numbers:

$$\frac{1}{n} \sum_i^n \exp\{\phi_{\beta_t}(x_{t,i})\} \xrightarrow{P} \mathbb{E}_{q_t}[\exp\{\phi_{\beta_t}(x)\}] \quad (23)$$

Because $q_t(x)$ and $q_{t-1}(x)$ are assumed independent, combine the above results we get:

$$\begin{aligned} \sqrt{n} \ell'_r(\beta_t^*) &\rightsquigarrow \mathcal{N}(\mu, \sigma^2), \\ \mu &= \sqrt{n} \left(\mathbb{E}_{q_{t-1}}[\nabla_{\beta_t} \phi_{\beta_t^*}(x)] - \frac{\mathbb{E}_{q_t}[\nabla_{\beta_t} \exp\{\phi_{\beta_t^*}(x)\}]}{\mathbb{E}_{q_t}[\exp\{\phi_{\beta_t^*}(x)\}]} \right), \\ \sigma^2 &= Cov_{q_{t-1}}[\nabla_{\beta_t} \phi_{\beta_t^*}(x)] + \frac{Cov_{q_t}[\nabla_{\beta_t} \exp\{\phi_{\beta_t^*}(x)\}]}{\mathbb{E}_{q_t}[\exp\{\phi_{\beta_t^*}(x)\}]^2} \end{aligned} \quad (24)$$

Taking derivatives from both sides of $1 = \int r_{s_t}^*(x) q_t(x) dx$:

$$\begin{aligned} 0 &= \nabla_{\beta_t} \mathbb{E}_{q_t}[r_{s_t}^*(x)] = \int \nabla_{\beta_t} r_{s_t}^*(x) q_t(x) dx \\ &= \int \frac{\nabla_{\beta_t} r_{s_t}^*(x)}{r_{s_t}^*(x)} r_{s_t}^*(x) q_t(x) dx \\ &= \int \nabla_{\beta_t} \log r_{s_t}^*(x) q_{t-1}(x) dx \\ &= \mathbb{E}_{q_{t-1}}[\nabla_{\beta_t} \log r_{s_t}^*(x)] \\ &= \mathbb{E}_{q_{t-1}}[\nabla_{\beta_t} \phi_{\beta_t^*}(x)] - \frac{\mathbb{E}_{q_t}[\nabla_{\beta_t} \exp\{\phi_{\beta_t^*}(x)\}]}{\mathbb{E}_{q_t}[\exp\{\phi_{\beta_t^*}(x)\}]} \end{aligned} \quad (25)$$

which gives $\mu = 0$. We prove the lemma. \square

Lemma 5. Let $\ell''_r(\beta_t^*) \triangleq \frac{1}{n} \sum_{j=1}^n \nabla_{\beta_t}^2 \log r_{s_t}(x_{t-1,j})|_{\beta_t=\beta_t^*}$, we have $\ell''_r(\beta_t^*) \xrightarrow{P} -I_{\beta_t^*}$, where $I_{\beta_t^*} \triangleq Cov_{q_{t-1}}[\nabla_{\beta_t} \phi_{\beta_t^*}(x)]$.

Proof. According to Eq. (20)

$$\begin{aligned} (\nabla_{\beta_t} \log r_{s_t}(x))^2 &= \left(\frac{\sum_i^n \nabla_{\beta_t} \exp\{\phi_{\beta_t}(x_{t,i})\}}{\sum_i^n \exp\{\phi_{\beta_t}(x_{t,i})\}} \right)^2 - \\ &\quad 2 \nabla_{\beta_t} \phi_{\beta_t}(x) \frac{\sum_i^n \nabla_{\beta_t} \exp\{\phi_{\beta_t}(x_{t,i})\}}{\sum_i^n \exp\{\phi_{\beta_t}(x_{t,i})\}} + (\nabla_{\beta_t} \phi_{\beta_t}(x))^2 \end{aligned} \quad (26)$$

By the law of large numbers,

$$\begin{aligned} \frac{1}{n} \sum_{j=1}^n (\nabla_{\beta_t} \log r_{s_t}(x_{t-1,j}))^2 &\xrightarrow{P} \left(\frac{\mathbb{E}_{q_t}[\nabla_{\beta_t} \exp\{\phi_{\beta_t}(x_{t,i})\}]}{\mathbb{E}_{q_t}[\exp\{\phi_{\beta_t}(x_{t,i})\}]} \right)^2 \\ &\quad - 2 \mathbb{E}_{q_{t-1}}[\nabla_{\beta_t} \phi_{\beta_t}(x)] \frac{\mathbb{E}_{q_t}[\nabla_{\beta_t} \exp\{\phi_{\beta_t}(x_{t,i})\}]}{\mathbb{E}_{q_t}[\exp\{\phi_{\beta_t}(x_{t,i})\}]} \\ &\quad + \mathbb{E}_{q_{t-1}}[(\nabla_{\beta_t} \phi_{\beta_t}(x))^2] \end{aligned} \quad (27)$$

Substituting Eq. (25) to the right side of the above equation, we can get:

$$\begin{aligned} \frac{1}{n} \sum_{j=1}^n (\nabla_{\beta_t} \log r_{s_t}(x_{t-1,j}))^2 &\Big|_{\beta_t=\beta_t^*} \xrightarrow{P} \\ &\quad \mathbb{E}_{q_{t-1}}[(\nabla_{\beta_t} \phi_{\beta_t^*}(x))^2] - \mathbb{E}_{q_{t-1}}[\nabla_{\beta_t} \phi_{\beta_t^*}(x)]^2 \\ &\quad = Cov_{q_{t-1}}[\nabla_{\beta_t} \phi_{\beta_t^*}(x)] = I_{\beta_t^*} \end{aligned} \quad (28)$$

Because

$$\nabla_{\beta_t}^2 \log r_{s_t}(x) = \frac{\nabla_{\beta_t}^2 r_{s_t}(x)}{r_{s_t}(x)} - (\nabla_{\beta_t} \log r_{s_t}(x))^2, \quad (29)$$

then according to Eq. (28)

$$\begin{aligned} \ell_r''(\beta_t^*) &\xrightarrow{P} \mathbb{E}_{q_{t-1}} \left[\frac{\nabla_{\beta_t}^2 r_{s_t}^*(x)}{r_{s_t}^*(x)} \right] - I_{\beta_t^*} \\ &= \int \nabla_{\beta_t}^2 r_{s_t}^*(x) q_t(x) dx - I_{\beta_t^*} \end{aligned} \quad (30)$$

Under mild assumptions we can interchange the integral and derivative operators:

$$\begin{aligned} \int \nabla_{\beta_t}^2 r_{s_t}^*(x) q_t(x) dx &= \nabla_{\beta_t}^2 \int r_{s_t}^*(x) q_t(x) dx \\ &= \nabla_{\beta_t}^2 \int \frac{q_{t-1}(x)}{q_t(x)} q_t(x) dx = 0 \end{aligned} \quad (31)$$

then we prove this lemma. \square

Lemma 6. Let $\ell_c(\beta_t) \triangleq \lambda_c \left(\frac{\Psi_t(x_t)}{\Phi_t(x_t)\Psi_{t-1}(x_{t-1})} - 1 \right)^2$, and $\ell_c'(\beta_t^*) \triangleq \nabla_{\beta_t} \ell_c(\beta_t)|_{\beta_t=\beta_t^*}$, if we set $\lambda_c = \frac{A}{\sqrt{n}}$, where A is a positive constant, then $\sqrt{n}\ell_c'(\beta_t^*) \xrightarrow{P} 0$.

Proof.

$$\begin{aligned} \sqrt{n}\ell_c'(\beta_t) &= 2A \left(\frac{\Psi_t(x_t)}{\Phi_t(x_t)\Psi_{t-1}(x_{t-1})} - 1 \right) \times \\ &\quad \left(\nabla_{\beta_t} \frac{\Psi_t(x_t)}{\Phi_t(x_t)\Psi_{t-1}(x_{t-1})} \right) \end{aligned}$$

By the law of large numbers,

$$\begin{aligned} \frac{\Psi_t(x_t)}{\Phi_t(x_t)\Psi_{t-1}(x_{t-1})} \Big|_{\beta_t=\beta_t^*} &\xrightarrow{P} \\ &\frac{\mathbb{E}_{q_t}[\exp\{\psi_{\beta_t^*}(x)\}]}{\mathbb{E}_{q_t}[\exp\{\phi_{\beta_t^*}(x)\}]\mathbb{E}_{q_{t-1}}[\exp\{\psi_{\beta_{t-1}}(x)\}]} \end{aligned}$$

Define $\tilde{r}_{t-1}(x) \triangleq \frac{\exp\{\psi_{\beta_{t-1}}(x)\}}{\mathbb{E}_{q_{t-1}}[\exp\{\psi_{\beta_{t-1}}(x)\}]}$, by the definition of $r_{s_t}^*(x)$ (Eq. (19)):

$$\begin{aligned} \int \tilde{r}_{t-1}(x) r_{s_t}^*(x) q_t(x) dx &= \int \tilde{r}_{t-1}(x) \frac{q_{t-1}(x)}{q_t(x)} q_t(x) dx \\ &= \int \tilde{r}_{t-1}(x) q_{t-1}(x) dx = 1 \end{aligned}$$

Substituting the right side of Eq. (19) into the left side of the above equation, we can get:

$$\frac{\mathbb{E}_{q_t}[\exp\{\psi_{\beta_t^*}(x)\}]}{\mathbb{E}_{q_t}[\exp\{\phi_{\beta_t^*}(x)\}]\mathbb{E}_{q_{t-1}}[\exp\{\psi_{\beta_{t-1}}(x)\}]} = 1 \quad (32)$$

then we prove this lemma. \square

Theorem 1. Suppose $\lambda_c = \frac{A}{\sqrt{n}}$, where A is a positive constant, assume $\ell_c'(\beta_t^*) = o_p(1)$, $\hat{\beta}_t - \beta_t^* = o_p(1)$, $\mathcal{L}_t'''(\tilde{\beta}_t) = O_p(1)$, where $\tilde{\beta}_t$ is a point between $\hat{\beta}_t$ and β_t^* , then $\sqrt{n}(\hat{\beta}_t - \beta_t^*) \rightsquigarrow \mathcal{N}(0, \mathbf{v}^2)$, where

$$\begin{aligned} \mathbf{v}^2 &= I_{\beta_t^*}^{-1} + \mathbb{E}_{q_t}[\exp\{\phi_{\beta_t^*}(x)\}]^{-2} \times \\ &\quad I_{\beta_t^*}^{-1} \text{Cov}_{q_t}[\nabla_{\beta_t} \exp\{\phi_{\beta_t^*}(x)\}] I_{\beta_t^*}^{-1} \end{aligned} \quad (33)$$

Proof. Applying Taylor expansion to Eq. (18) around β_t^* :

$$\begin{aligned} 0 &= \mathcal{L}_t'(\hat{\beta}_t) = \mathcal{L}_t'(\beta_t^*) + (\hat{\beta}_t - \beta_t^*) \mathcal{L}_t''(\beta_t^*) \\ &\quad + \frac{1}{2}(\hat{\beta}_t - \beta_t^*)^2 \mathcal{L}_t'''(\tilde{\beta}_t), \\ \sqrt{n}(\hat{\beta}_t - \beta_t^*) &= \frac{-\sqrt{n}\mathcal{L}_t'(\beta_t^*)}{\mathcal{L}_t''(\beta_t^*) + \frac{1}{2}(\hat{\beta}_t - \beta_t^*) \mathcal{L}_t'''(\tilde{\beta}_t)} \end{aligned} \quad (34)$$

where

$$\mathcal{L}_t(\beta_t) = \ell_r(\beta_t) + \ell_c(\beta_t) \quad (35)$$

As we assume $\ell_c'(\beta_t^*) = o_p(1)$, according to Lemma 5, we get $\mathcal{L}_t''(\beta_t^*) \xrightarrow{P} -I_{\beta_t^*}$. Combine the results of Lemmas 4 and 6 we prove the theorem. \square

Corollary 1. Suppose $p(x)$ and $\forall t, q_t(x)$ are from the exponential family, define $r_{s_t}^*(x) = \exp\{\phi_{\beta_t^*}(x)\}$, $\phi_{\beta_t^*}(x) = \beta_t^* T(x) + C$, $T(x)$ is a sufficient statistic of x , C is a constant, then $\sqrt{n}(\hat{\beta}_t - \beta_t^*) \rightsquigarrow \mathcal{N}(0, \mathbf{v}_e^2)$, where $T(x)$ is a column vector; $T(x)^2 = T(x)T(x)^T$, $I_{\beta_t^*} = \text{Cov}_{q_{t-1}}[T(x)]$:

$$\mathbf{v}_e^2 = I_{\beta_t^*}^{-1} + I_{\beta_t^*}^{-1} (\mathbb{E}_{q_{t-1}}[r_{s_t}^*(x)T(x)^2] - \mathbb{E}_{q_{t-1}}[T(x)]^2) I_{\beta_t^*}^{-1} \quad (36)$$

Proof. Because $\phi_t^*(x) \triangleq \psi_{\beta_t^*}(x) - \psi_{\beta_{t-1}^*}(x)$, then $\nabla_{\beta_t} \phi_{\beta_t^*}^*(x) = T(x)$, we have

$$I_{\beta_t^*} = \text{Cov}_{q_{t-1}}[\nabla_{\beta_t} \phi_{\beta_t^*}^*(x)] = \text{Cov}_{q_{t-1}}[T(x)], \quad (37)$$

Because $r_{s_t}^*(x) = \exp\{\phi_{\beta_t^*}^*(x)\}$,

$$\mathbb{E}_{q_t}[\exp\{\phi_{\beta_t^*}^*(x)\}] = \mathbb{E}_{q_t}[r_{s_t}^*(x)] = 1,$$

In addition,

$$\begin{aligned} \text{Cov}_{q_t}[\nabla_{\beta_t} \exp\{\phi_{\beta_t^*}^*(x)\}] &= \text{Cov}_{q_t}[r_{s_t}^*(x)T(x)] \\ &= \mathbb{E}_{q_t}[(r_{s_t}^*(x)T(x))^2] - \mathbb{E}_{q_t}[r_{s_t}^*(x)T(x)]^2 \end{aligned} \quad (38)$$

where

$$\begin{aligned} \mathbb{E}_{q_t}[(r_{s_t}^*(x)T(x))^2] &= \int q_t(x) (r_{s_t}^*(x)T(x))^2 dx \\ &= \int q_{t-1}(x) r_{s_t}^*(x) T(x)^2 dx = \mathbb{E}_{q_{t-1}}[r_{s_t}^*(x)T(x)^2], \\ \mathbb{E}_{q_t}[r_{s_t}^*(x)T(x)] &= \int q_t(x) r_{s_t}^*(x) T(x) dx \\ &= \int q_{t-1}(x) T(x) dx = \mathbb{E}_{q_{t-1}}[T(x)] \end{aligned} \quad (39)$$

Substitute above results into Theorem 1, we prove the corollary. \square

B Experimental settings

We elaborate the experimental settings of the ratio estimators, feature generators, and GANs in our experiments here. The source code will be made public upon acceptance.

B.1 Configuration of ratio estimators

The ratio estimator we used in all experiments is the log-linear model as defined in Eq. 9 of Sec. 3, and $\psi(\cdot)$ is a neural network with two dense layers, each having 256 hidden units. It is trained by Adam optimizer, and batch size is 2000, learning rate is 10^{-5} . λ_c is 10 and $100k$ for the single and multiple original distributions, respectively, where k is the number of joined original distributions.

B.2 Configuration of feature generators

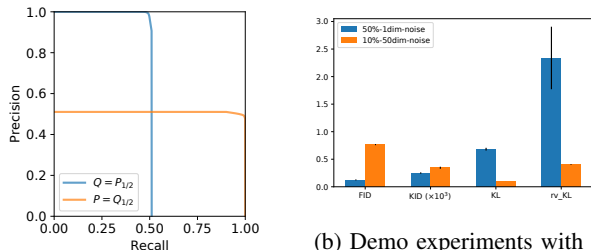
The classifier used to extract features on both datasets has two convolutional layers with filter shape [4,4,1,64], [4,4,64,128] respectively, strides are all [1,2,2,1], and two dense layers with 6272 and 64 hidden units respectively. Batch normalization is performed on the second convolutional layer and the first dense layer. The encoder of the CVAE has two dense layers with 512 and 256 hidden units respectively, output dimension is 64. The decoder has two dense layers each with 256 hidden units, output dimension is 784. Activation function of all hidden layers is ReLU. Both feature generators are trained with L2 regularization.

B.3 Configuration of GANs

All GANs are trained with a discriminator having the same architecture as the classifier described above, except the last dense layer has 1024 hidden units; a generator having two convolutional layers with filter shape [4,4,64,128] and [4,4,1,64], respectively, two dense layers with 1024 and 6272 hidden units respectively, batch normalization is applied to two dense layers. Activation function is leaky ReLU (Xu et al., 2015) for all hidden layers. All GANs are trained by Adam optimizer, batch size is 64, learning rate is 0.0002 and 0.001 for the discriminator and generator respectively. The random input of the generators has 64 dimensions for both MNIST and Fashion-MNIST tasks.

C Evaluating generative models using f -divergences

We compare f -divergences with FID (Heusel et al., 2017), KID (Bińkowski et al., 2018) and PRD (Sajjadi et al., 2018) in several experiments with toy data and a high-dimensional dataset of the real world. Through these experiments, we show that f -divergences can be effective measures of generative models and one may obtain richer criteria by them.



(a) PRD of the demo experiment in Tab. 1

(b) Demo experiments with different types of noise injected into MNIST (error bars from 5 runs).

Figure 7: Experimental results of demo experiments

C.1 Demo experiments with MNIST

We present demo experiments to show the differences between f -divergences and FID, KID in terms of evaluating generative models. We demonstrate the experiment results through two most popular members of f -divergences: KL-divergence and reverse KL-divergence.

In the first experiment, We have two cases: (i) the compared distribution P contains half of the classes of MNIST, and the evaluated distribution Q includes all classes of MNIST; (ii) the reverse of (i). We obtain density ratios by KLIEP and then estimate f -divergences by the ratios. The results are shown in Tab. 1, with PRD curves displayed in Fig. 7a. Since the objective of KLIEP is not symmetric, the estimated KL divergences are not symmetric when switching the two sets of samples. As we can see, $D_{KL}(P||Q)$ prefers Q with larger recall and vice versa. Neither FID nor KID are able to discriminate between these two scenarios.

In the second experiment, we show that f -divergences may provide different opinions with FID and KID in certain circumstances because FID and KID are based on IPM (Sriperumbudur et al., 2012) which focus on parts with the most probability mass whereas f -divergences are based on density ratios which may give more attention on parts with less probability mass (due to the ratio of two small values can be very large). To show this, we simulate two sets of noisy samples by injecting two different types of noise into MNIST data and evaluate them as the model samples on the pixel feature space (which is 784 dimensions). Regarding the first type of noise, we randomly choose 50% samples and 1 dimension to be corrupted (set the pixel value to 0.5); for the second one, we randomly choose 10% samples and 50 dimensions to be corrupted. The results are shown in Fig. 7b, in which KL-divergence and reverse KL-divergence disagree with FID and KID regarding which set of samples is better than the other.

Table 1: Results of the first demo experiment. $P = Q_{1/2}$ implies case (i), $Q = P_{1/2}$ implies case (ii). Standard deviations are from 5 runs.

	FID	KID	$D_{KL}(P Q)$	$D_{KL}(Q P)$
$P = Q_{1/2}$	50.39 ± 0.00	2.04 ± 0.01	0.67 ± 0.00	3.78 ± 1.22
$Q = P_{1/2}$	50.39 ± 0.00	2.03 ± 0.02	2.49 ± 0.30	2.38 ± 1.78

C.2 Evaluating on high-dimensional data by f -divergences

In order to show that f -divergences can work with high-dimensional data as the same as FID and KID, we also conducted an experiment with samples of StyleGAN¹ trained by FFHQ dataset (Karras et al., 2019). We estimate f -divergences on the inception feature space with 2048 dimensions. The sample size is 50000 and we compare the model samples with real samples. We see that the f -divergences give reasonable results with small variance (Tab. 2), indicating it is capable of evaluating generative models with high dimensional data.

Table 2: Evaluating StyleGAN on FFHQ dataset using f -divergences

	StyleGAN	Real samples
KL	2.47 ± 0.02	$0.02 \pm 9.1e-4$
rv_KL	3.29 ± 0.18	$0.02 \pm 9.3e-4$
JS	0.86 ± 0.01	$0.01 \pm 4.5e-4$
Hellinger	1.04 ± 0.02	$0.01 \pm 4.6e-4$

D Experiment results on MNIST

We show experiment results on MNIST in Figs. 8 and 9, the settings of these experiments are the same as experiments with Fashion-MNIST.

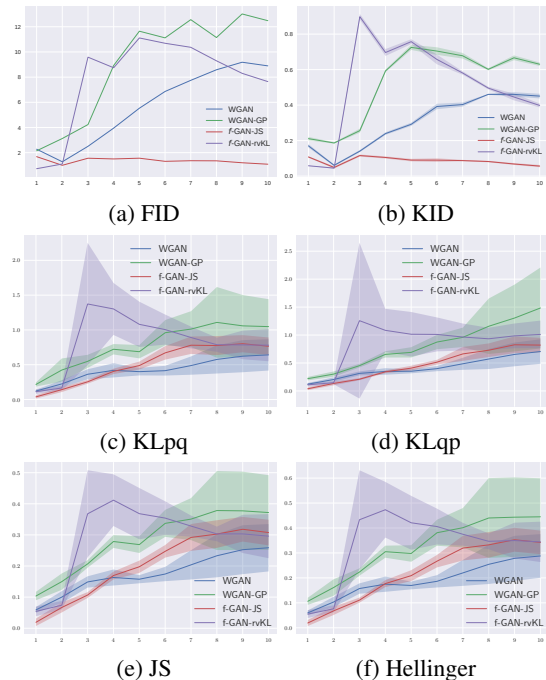


Figure 8: Evaluating GANs in continual learning on MNIST, features for FID and KID are extracted from the classifier, features for f -divergences are generated by CVAE. The shaded area are plotted by standard deviation of 10 runs.

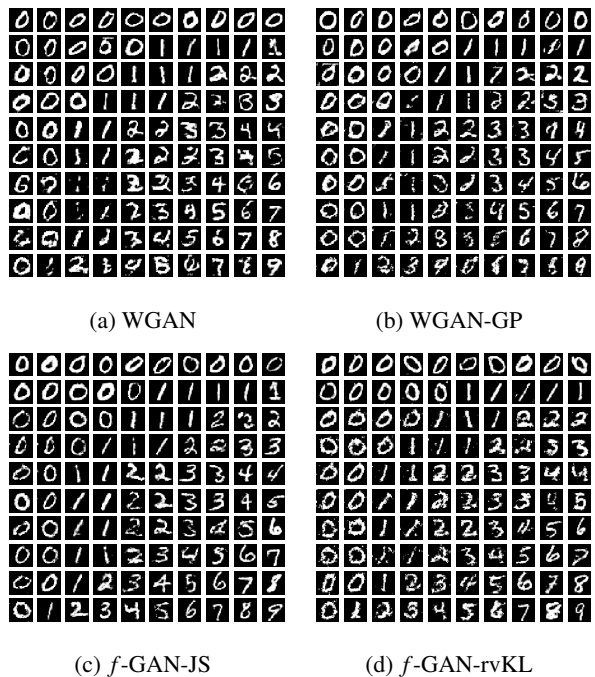


Figure 9: MNIST samples generated by evaluated GANs in continual learning. In each figure, each row displays figures generated at each task, the order is from the top to bottom.

¹<https://github.com/NVlabs/stylegan>